საქართველოს მეცნიერებათა ეროვნული აკადემიის მოამბე, ტ. 19(193), №3, 2025
BULLETIN OF THE GEORGIAN NATIONAL ACADEMY OF SCIENCES, vol. 19(193), no. 3, 2025

Physics

Design Study of the Proton Beam Position Monitor for the Hadron Center at Kutaisi International University

Shalva Bilanishvili

Kutaisi International University, Kutaisi Hadron Center, Georgia

(Presented by Academy Member Alexander Kvinikhidze)

Abstract. Cyclotron-based proton beams are widely used in research with medical applications due to their capability to deliver bunched beams with a broad range of bunch charges. One of the most critical components in beam diagnostics is the beam position monitor (BPM), which must accurately measure the beam's position while minimizing disturbance to the beam. At Kutaisi International University (KIU), a superconducting synchro-cyclotron (S2C2) provided by Ion Beam Applications (IBA) will be dedicated exclusively to research, supporting diverse experiments that benefit from proton bunched beams of different intensities. To accommodate these experiments, the construction of a compact beamline is planned. In this work, we present the electromagnetic design study of an electrostatic BPM that can operate effectively within the physical and operational constraints of a new beamline. © *2025 Bull. Georg. Natl. Acad. Sci.*

Keywords: beam position monitors, simulations, cyclotrons

Introduction

Beam Position Monitors (BPMs) are crucial diagnostic tools to effectively manipulate particle beams, by providing precise beam position. However, achieving sufficient signal levels from low-intensity bunched beams can be challenging. The minimum beam current for which a BPM yields usable position information (the detection threshold) is fundamentally limited by electronic readout noise and manufacturing errors.

In the case of the IBA superconducting synchro-cyclotron (S2C2) (Kleeven et al., 2013, Pearson et al., 2013) at Kutaisi International University (KIU), the extracted proton beam consists of short pulses $\sim \mu s$ at a repetition rate of ~ 1 kHz. The average extracted beam current is of the order of only a few tens of nano amperes. These parameters correspond to low bunch charges (of the order of 10^{-11} to 10^{-10} C per pulse) and pose a significant challenge for beam position detection.

Capacitive pickups (button-style BPMs) are a convenient choice for this application due to their simplicity, compactness, and ultrahigh vacuum compatibility. A capacitive BPM consists of conductive 'button' electrodes mounted flush with the beam pipe inner wall. As a charged bunch passes, image charges are induced on the buttons, generating a voltage signal proportional to a fraction of the displacement and intensity of the beam. The fraction of the image current of the beam intercepted by a given button (and therefore the signal amplitude) depends on the electrode size, the position of the beam relative to it, and the transfer impedance (Marcellini et al., 1998).

This work presents a simulation-based design study of a capacitive BPM for the S2C2 beamline at KIU. The goal is to determine the optimal button electrode size that yields the sufficient sensitivity to beam position across the expected range of bunch charges and offsets. Sensitivity here refers to the BPM's output voltage response per unit of beam displacement and charge. The study is conducted by simulation tools, therefore we focus on studying trends and identifying a viable design range.

General Considerations

Table. General parameters for IBA S2C2 (Pearson et al., 2013)

Parameter	Description	Value
Size	yoke/pole radius weight	1.25 m/ 0.5 m 50 tons
Magnetic field	central/extraction	5.7 T/ 5.0 T
Beam pulse	rate/length	1000 Hz/ 7 μ s
RF system	frequency	93 - 63 MHz
	voltage	10 kV
Maximum energy		250 MeV

The button electrode primarily responds to the electric field of the beam. An electrostatic monitor can typically be represented by an equivalent circuit that includes a current generator with the same value as the fraction of intercepted image current, which is then shunted by the electrode capacitance to ground. To connect the button to the detector circuit, a short length of modified coaxial cable with a characteristic impedance of R_0 is used, and an R_0 resistor terminates it.

It is worth noting that the circuit model delivers satisfying results with only minor corrections necessary for a circular button geometry and relativistic beam velocities, i.e., TEM-like (transverse electromagnetic) field pattern. If the beam is accelerated to a non-relativistic velocity, $\beta \ll 1$, as for cyclotrons, the electric field cannot be described by a TEM wave anymore. Instead, the field pattern has a significantly longitudinal extension because the electric field propagation is faster than the beam velocity (Shafer, 1994). However, for higher beam velocities, i.e., for $\beta \geq 0.3$, the electric charge distribution squeezes approaching a layer TEM wave, so the circuit model should provide good approximation in our case (Shafer, 1992, Kowina et al., 2009).

When the beam is centered, the transfer impedance, which is the complex ratio of the voltage induced by the beam at the external termination to the beam current, can be expressed as:

$$Z_b(\omega) = \phi R_0 \left(\frac{\omega_1}{\omega_2}\right) \frac{j\omega/\omega_1}{1 + j\omega/\omega_1}, \ \mathrm{Re}Z_b(\omega) = \phi R_0 \left(\frac{\omega_1}{\omega_2}\right) \frac{(\omega/\omega_1)^2}{1 + (\omega/\omega_1)^2},$$

$$\mathrm{Im}Z_b(\omega) = \phi R_0 \left(\frac{\omega_1}{\omega_2}\right) \frac{\omega/\omega_1}{1 + (\omega/\omega_1)^2},$$

here, by the frequencies ω_1 and ω_2 represent: $\omega_1 = 1/R_0 C_b$ and $\omega_2 = c/2r$, where C_b is the button capacitance to ground, r is the radius of the button, c is the speed of light, and b is the radius of the beam pipe. The coverage factor, ϕ, is also defined in terms of r and b, as $\phi = r/4b$ (Bilanishvili et al., 2024).

The frequency response is classified as high-pass, and two separate regimes can be distinguished for low frequency $(\omega \ll \omega_1)$ and high frequency $(\omega \gg \omega_1)$, respectively:

$$Z_{b(\omega \ll \omega_1)} = \phi R_0 \frac{j\omega}{\omega_2} = j\omega R_0 \left(\frac{r^2}{2bc} \right)$$

$$Z_{b(\omega \gg \omega_1)} = \phi R_0 \left(\frac{\omega_1}{\omega_2} \right) = \frac{r^2}{2bcC_b} \ .$$

At low frequencies, the electrode behaves like a time differentiator. The transfer impedance mainly depends on the load resistance R_0 and geometrical factors b and r, and is largely unaffected by the capacitance C_b.

At high frequencies, the response is purely resistive, meaning that the electrode voltage is proportional to and in phase with the beam current. The transfer impedance scales inversely with the button capacitance and depends on the same geometrical factors, but not on R_0.

It is possible to shape the response for a given frequency range by adjusting the load resistor. For instance, increasing the value of the load resistor shifts the corner frequency ω_1 towards a lower value, thus extending the low-frequency response, without affecting the high-frequency response as long as the capacitance remains the same. To enhance the response at high frequencies, the capacitance can be reduced, but this causes the corner frequency ω_1 to shift towards a higher value, which is a drawback.

The absolute value of the transfer impedance,

$$\left| Z_b(\omega) \right| = \phi R_0 \left(\frac{\omega_1}{\omega_2} \right) \frac{\omega / \omega_1}{\sqrt{1 + (\omega / \omega_1)^2}} \ ,$$

increases quadratically with the button radius, making a larger radius preferable for higher sensitivity across all frequencies. Enhancing the electrode surface improves the overall response, but increasing capacitance reduces the response at high frequency, while decreasing capacitance has the opposite effect. To reduce the low-frequency corner of the differentiator response, the load resistor value must be increased. However, these parameters are interdependent, increasing the radius may result in a linear or quadratic increase in capacitance, depending on the design. It is not feasible to increase the button radius beyond a certain limit, as the longitudinal coupling impedance scales as r^4,

$$Z_l(\omega) = \phi \left(\frac{\omega_1}{\omega_2} \right) Z_b \ .$$

The expression underestimates the coupling impedance, as it only considers the fields that contribute to the output signal formation. Numerical simulations have revealed other modes that do not dissipate their power in the external termination, such as the TE_{11}-like mode (transverse electric), which has a wavelength close to the mean perimeter of the annular cut created by the button and beam pipe walls. A smaller button radius is required to shift the frequency of the first parasitic mode towards higher frequencies, avoiding high power losses in the button BPM. The annular cut also contributes to the coupling impedance, which can be estimated analytically at low frequencies,

$$Z_{lcut}(\omega) = j \frac{Z_0 \omega (r + w)^3}{8cb^2 \left\{ ln\left[32(r + w)/w \right] - 2 \right\}} \ .$$

The coupling impedance is heavily dependent on the button radius, as evidenced in the last equation, where Z_0 represents the free space impedance, and by w size of the gap between the button and vacuum chamber wall is denoted.

Modelling and Simulations

The layout of the simulated BPM structures is displayed in Fig. 1. The structure consists of the button electrode, vacuum chamber, and the part that adjusts from button electrodes to the coaxial line.

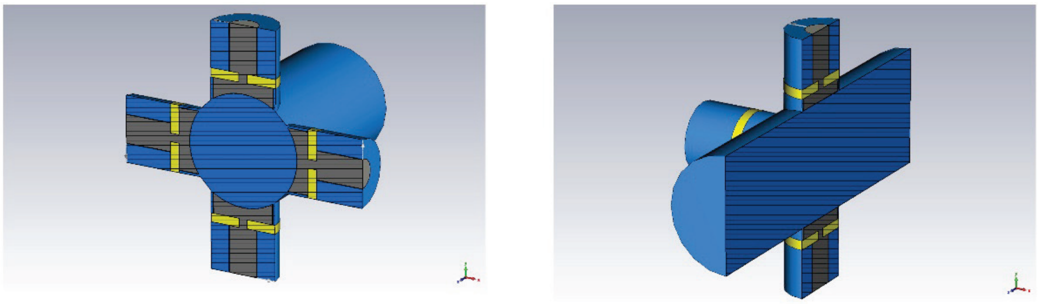

Fig. 1. Different perspectives of the structure for the wakefield simulations.

Each button electrode has a radius of 14 mm at the annular cut with the vacuum chamber and a gap of 1 mm with the beampipe wall. The bunch length used in the wakefield (When a charged particle travels across the vacuum chamber of an accelerator, it induces electromagnetic fields, which are left mainly behind the generating particle. These electromagnetic fields act back on the beam and influence its motion and are called wakefields.) simulations is 30 mm traveling along the structure's central axis. The BPM coaxial parts match the impedance of a 50 Ohms. A glass ring for vacuum insulation is located near the button region. It has a dielectric constant of about 6. The figures of the structure included in this paper are original, produced by the author and used as the geometry for all simulations carried out in this study.

The simulations are done in the time and frequency domains, which consists of two kinds of calculations, namely wakefield and port transmission calculations respectively.

In the wakefield calculation, a Gaussian beam is introduced in the z-direction, leading to the generation of electromagnetic fields at the BPM structure (Forck et al., 2009). These fields then influence the particle beam. To prevent the reflection of electromagnetic waves at the beam entrance and exit planes, waveguide boundary conditions are imposed. At the end boundary of the coaxial line, an outgoing waveguide port is considered to determine signal transmission.

To evaluate the coupling impedance of a button, one can either use the wakefield or its Fourier transform. The latter allows us to identify potential resonant modes that the particle bunch excites in the BPM. The resolution of narrow resonances in the impedance spectrum is directly proportional to the number of sampling points used in the wakefield calculation (Wendt, 2018). Therefore, we compute the wakefield up to s = 3 m, where s represents the bunch coordinate.

In order to estimate the transfer and coupling impedance of the button we have simulated structure also with the measurement method based on a coaxial wire put along with the beam tube.

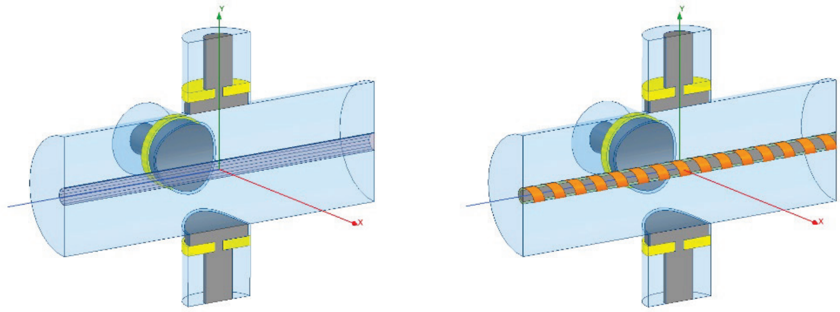

Fig. 2. Left: wire structure; right: helix structure.

Figure 2 displays the geometries used in the simulations to calculate the S-parameters. Two different methods were employed: simulations with only wire and with wire that is wrapped by conducting helix, to mimic the lower beta field patterns (Wang et al., 2024). The transfer impedance vs frequency can be found from the values of the scattering matrix elements. By computing the transfer impedance at the coaxial line port as a function of frequency, we can determine the signal strength picked up by the BPM as the beam traverses the corresponding section of the vacuum chamber (ANSYS Inc., n.d., Dassault Systèmes, n.d.). The images of the structure are original, produced by the author and used as the geometry for all simulations carried out in this study.

Results

Figure 3 presents comparison of the transfer impedance Z_b and S parameters for the structures with wire and helix respectively. Figure 4 shows the real imaginary parts of the longitudinal beam-coupling impedance $Z_{\parallel}(\omega)$ obtained from the wakefield simulation over the 0-20 GHz range. A broad inductive plateau is observed up to about 2.5 GHz; above which a series of narrow resonances becomes visible. The first pronounced higher-order mode (HOM) appears at f ≃ 2.8 GHz with a peak impedance of ≈ 60 Ω. Higher modes at 4.8 GHz and 9.9 GHz exhibit successively lower coupling impedances.

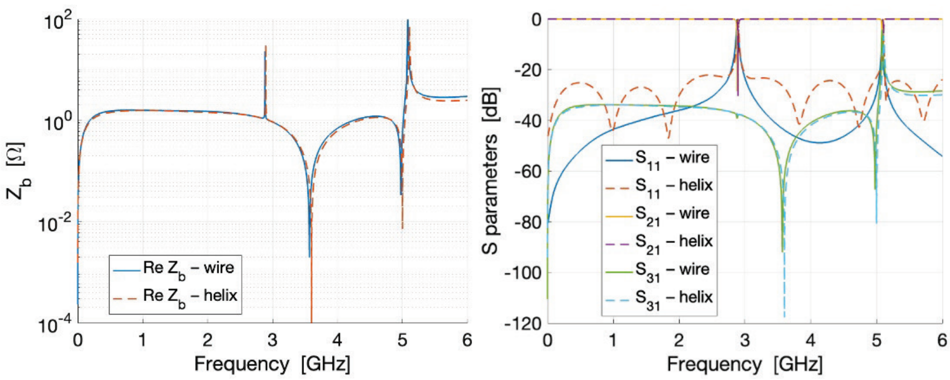

Fig. 3. Left: transfer impedance comparison for the wire and helix structures; right: different S-parameter comparison for wire and helix structures.

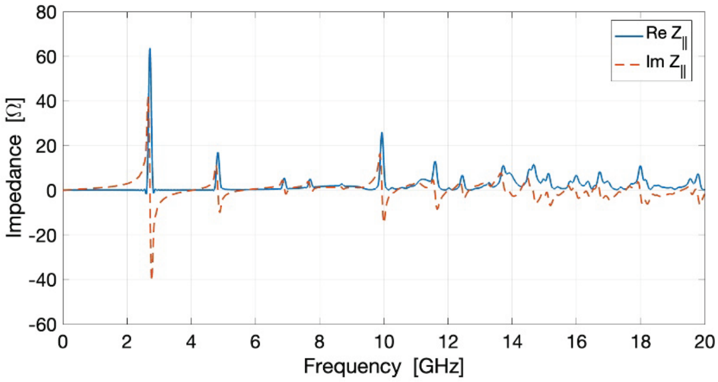

Fig. 4. Real and imaginary parts of the beam coupling impedance.

To compare the wakefield results, the structure was also simulated with the classical stretched-wire method and with a wire wrapped in a conducting helix to emulate sub-relativistic field patterns. Figure 4 shows the real part of longitudinal beam-coupling impedance up to first trapped higher-order mode, 2.5GHz on a logarithmic scale for:

- wakefield post-processing (solid blue);
- wire technique (dashed red).

The curves overlap within acceptable tolerance over the entire band.

Finally, Figure 6 displays a two-dimensional map of the BPM vertical Δ/Σ output voltage as a function of beam offset (-10 mm $\leq$ y $\leq$ 10 mm. The contours are nearly linear within $\pm$ 4 mm.

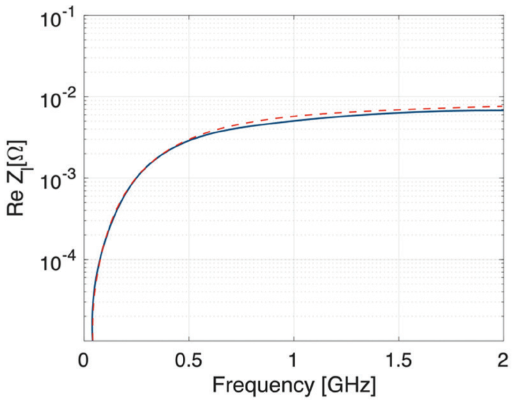

Fig. 5. Comparison of real part of the beam coupling impedance calculated by wakefield simulations and from S-parameters.

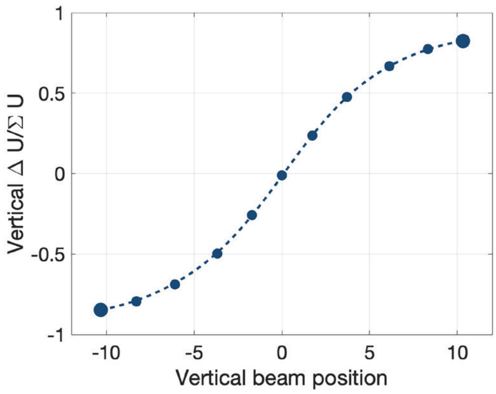

Fig. 6. Reconstructed vertical beam position calculated using ‘delta-over-sum’ algorithm from signal registered in vertical buttons for zero horizontal beam displacement.

Conclusion

The simulations based on finite element methods are very helpful to test different BPM approaches. A 3-dimensional visualization of the field propagation allows to understand complex processes which simplifies optimization of BPM design. Button electrodes with 14 mm radius for the 25 mm radius vacuum chamber can deliver sufficient position sensitivity for provided proton beams.

Acknowledgements

The work has been supported by the Shota Rustaveli National Science Foundation of Georgia: SRNSFG grant No. FR-22-8306.

ფიზიკა

პროტონული სხივის პოზიციის მონიტორის დიზაინის შესწავლა ქუთაისის საერთაშორისო უნივერსიტეტის ადრონული ცენტრისთვის

 შ. ბილანიშვილი

ქუთაისის საერთაშორისო უნივერსიტეტი, ქუთაისის ადრონული ცენტრი, საქართველო

(წარმოდგენილია აკადემიის წევრის ა. კვინიხიძის მიერ)

ციკლოტრონის მიერ გენერირებული პროტონული სხივები ფართოდ გამოიყენება კვლევითი და სამედიცინო დანიშნულებით, მათ მიერ ფართო დიაპაზონში ცვალებადი მუხტის მქონე პულსირებული ნაკადის მიწოდების უნარის გამო. სხივის დიაგნოსტიკის ერთ-ერთი მნიშვნელოვანი კომპონენტია სხივის პოზიციის მონიტორი (BPM), რომელმაც ზუსტად უნდა გაზომოს სხივის პოზიცია და, ამავდროულად, მინიმუმამდე დაიყვანოს სხივის შეშფოთება. ქუთაისის საერთაშორისო უნივერსიტეტში (KIU), Ion Beam Applications (IBA)-ს მიერ მოწოდებული ზეგამტარი სინქროციკლოტრონი (S2C2) ექსკლუზიურად კვლევითი ამოცანებისთვის იქნება განკუთვნილი და მოემსახურება განსხვავებული ინტენსივობის პროტონული სხივების გამოყენებით ჩატარებულ სხვადასხვა ექსპერიმენტს. ამ ექსპერიმენტების ჩასატარებლად დაგეგმილია კომპაქტური სხივური არხის აშენება. წინამდებარე ნაშრომში წარმოდგენილია ელექტროსტატიკური BPM-ის ელექტრომაგნიტური დიზაინის კვლევა, რომელიც ეფექტურად იმუშავებს და შეესაბამება ახალი სხივური არხის ფიზიკურ და ოპერაციულ შეზღუდვებს.

REFERENCES

ANSYS Inc. (n.d.). *Ansys HFSS* [Computer software]. https://www.ansys.com/products/electronics/ansys-hfss

Bilanishvili, S., et al. (2024). Capacitive BPM electromagnetic design optimisation. *Journal of Physics: Conference Series, 2687*, 072004. https://doi.org/10.1088/1742-6596/2687/7/072004

Dassault Systèmes. (n.d.). *CST Studio Suite* [Computer software]. https://www.cst.com/

Forck, P., et al. (2009). Beam position monitors. In *CAS – CERN Accelerator School: Beam diagnostics* (p. 187). CERN. https://doi.org/10.5170/CERN-2009-005.187

Kleeven, W., et al. (2013, September). The IBA superconducting synchrocyclotron project S2C2. In *Proceedings of Cyclotrons 2013* (pp. 115–117). Paper MO4PB02.

Kowina, P., et al. (2009, May). FEM simulations – a powerful tool for BPM design. In *Proceedings of DIPAC 2009* (pp. 35-37). Paper MOOC03.

Marcellini, F., et al. (1998). DAΦNE broad-band button electrodes. *Nuclear Instruments and Methods in Physics Research Section A: Accelerators, Spectrometers, Detectors and Associated Equipment, 402*, 27-35. https://doi.org/10.1016/S0168-9002(97)01083-8

Pearson, E., et al. (2013, August 5–8). The new IBA superconducting synchrocyclotron (S2C2): From modeling to reality. In *Proceedings of the 11th International Topical Meeting on Nuclear Applications of Accelerators (AccApp '13)*.

Shafer, R. E. (1992). Beam position monitoring. *AIP Conference Proceedings, 249*, 601-636. https://doi.org/10.1063/1.41980

Shafer, R. E. (1994). Beam position monitor sensitivity for low-β beams. *AIP Conference Proceedings, 319*, 303-308. https://doi.org/10.1063/1.46975

Wang, M., et al. (2024, September). Progress of low-β BPM calibration based on helical slow-wave structure. In *Proceedings of IBIC 2024* (pp. 142-144). Paper TUP40. https://doi.org/10.18429/JACoW-IBIC2024-TUP40

Wendt, M. (2018). BPM systems: A brief introduction to beam position monitoring [Preprint]. *arXiv*. https://doi.org/10.48550/arXiv.2005.14081

Received June, 2025